Femtolitre Volume cryoEM Sample Preparation Using a Force-Sensitive Microfluidic Cantilever

Shastri, Vijayendra; Pronk, Joachim; Verlinden, Eleonoor; González, Daniel Torres; Sarajlic, Edin; Laeven, Paul; Evers, Wiel; Frederix, Patrick; Staufer, Urs; Jakobi, Arjen J.

DOI
10.1002/admt.202501333

Publication date
2025

Document Version
Final published version

Published in
Advanced Materials Technologies

Citation (APA)
Shastri, V., Pronk, J., Verlinden, E., González, D. T., Sarajlic, E., Laeven, P., Evers, W., Frederix, P., Staufer, U., Jakobi, A. J., Ghatkesar, M. K., & Engel, A. (2025). Femtolitre Volume cryoEM Sample Preparation Using a Force-Sensitive Microfluidic Cantilever. *Advanced Materials Technologies*, Article e01333. https://doi.org/10.1002/admt.202501333

ADVANCED MATERIALS TECHNOLOGIES
www.advmattechnol.de

Femtolitre Volume cryoEM Sample Preparation Using a Force-Sensitive Microfluidic Cantilever

Vijayendra Shastri, Joachim Pronk, Eleonoor Verlinden, Daniel Torres González, Edin Sarajlic, Paul Laeven, Wiel Evers, Patrick Frederix, Urs Staufer, Arjen J. Jakobi, Murali Krishna Ghatkesar,* and Andreas Engel*

Cryogenic electron microscopy (cryoEM) has become an indispensable technique for determining the structures of isolated biological macromolecules and imaging biomolecular structures within cells. While thin films of frozen-hydrated macromolecule suspensions can be directly prepared and imaged, these molecules must be extracted from their cellular context using existing sample preparation methods. On the other hand, cellular specimens preserve the native context, but the region of interest must be sectioned or subjected to focused ion-beam milling at cryogenic temperatures to achieve the necessary thickness for transmission electron imaging. Currently, no method exists for targeted cytoplasmic extraction of a subcellular volume from individual cells for direct vitrification and cryoEM imaging. In this study, a method is presented that addresses this gap. A system has developed that utilizes a force-sensitive microfluidic cantilever pipette to aspirate and dispense sample volumes as small as 204 fL onto conventional cryoEM sample supports, maintained at the dew point. This is followed by automatic vitrification for cryoEM imaging. Coupled with a fluorescence microscope, this setup allows for the extraction of a targeted subcellular volume from an individual cell and subsequent dispensing of the aspirated content onto an electron microscopy grid. A proof-of-concept is demonstrated by dispensing femtolitre volumes of the standard cryoEM single-particle sample, tobacco mosaic virus, and performing a subcellular biopsy from a single HeLa cell. Additionally, the challenges of manipulating such small volumes for cryoEM sample preparation are discussed, highlighting the current limitations of this approach and potential solutions for overcoming them.

1. Introduction

Cryogenic electron microscopy (cryoEM) has become an indispensable technique for structural studies of biological macromolecules.[1–3] Central to the success of cryoEM is the sample preparation process, which aims to preserve the native state of biological molecules and cellular complexes.[4] Over the years, advancements in cryoEM sample preparation methods have played a pivotal role in enhancing the quality and efficiency of cryoEM studies.[5–8] Recent developments have increased the level of automation in cryoEM sample and reduced the required sample volumes to nanolitres (Refs. [9–12] or even picolitres Ref. [13])

At present, most structural studies with cryoEM rely on purifying complexes from the cell for high-resolution imaging. While successful, this approach is typically reserved for samples with limited biochemical complexity. In addition, the absence of essential interaction partners and/or native post-translational modifications might lead to non-physiological conformations or oligomeric states, and their

V. Shastri, E. Verlinden, D. T. González, U. Staufer, A. J. Jakobi, M. K. Ghatkesar
Department of Precision and Microsystems Engineering
Delft University of Technology
Mekelweg 2, Delft 2628 CD, The Netherlands
E-mail: a.jakobi@tudelft.nl; m.k.ghatkesar@tudelft.nl

J. Pronk, W. Evers, A. Engel
Department of Bionanoscience
Kavli Institute for Nanoscience
Delft University of Technology
Van der Maasweg 9, Delft 2629 HZ, The Netherlands

E. Sarajlic
SmartTip BV
De Veldmaat 17, Enschede 7522 NM, The Netherlands

P. Laeven
Maastricht University
Minderbroedersberg 4-6, Maastricht 6211 LK, The Netherlands

P. Frederix
Nansosurf AG
Gräubernstrasse 12/14, Liestal 4410, Switzerland

The ORCID identification number(s) for the author(s) of this article can be found under https://doi.org/10.1002/admt.202501333

DOI: 10.1002/admt.202501333

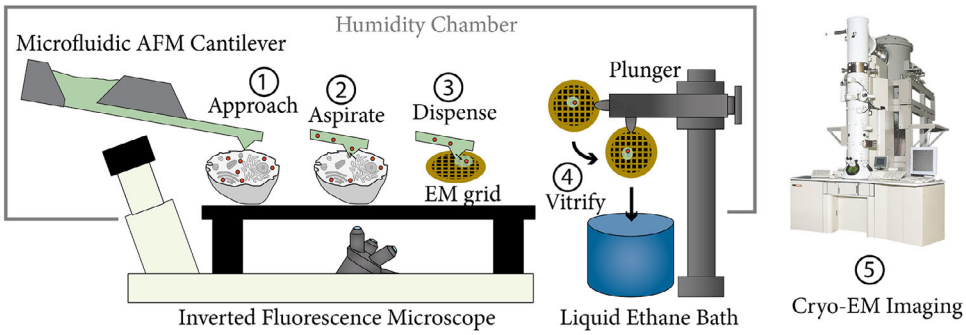

Figure 1. Schematic representation of using a microfluidic atomic force microscopy cantilever for cryoEM sample preparation, AFM4cryoEM. 1) A microfluidic AFM cantilever filled with buffer (light-green color) approaches the cell and 2) penetrates to aspirate fluorescently labelled target contents inside a single cell (red colored spheres). Aspirated subcellular biopsy content is dispensed onto a TEM grid 3) that is eventually plunged into liquid ethane 4) for vitrification. The entire sample preparation setup is maintained at 70% relative humidity and the TEM grid is held just above dew point temperature to minimise evaporation of the sample on the grid before plunging. The vitrified sample is then imaged by cryogenic electron microscopy 5).

spatiotemporal modulation may remain elusive when taken out of cellular context. Structural information on cellular ultrastructure and the cell's macromolecular machinery obtained in their native context can be invaluable for understanding their assembly and mechanism. Recent technological advances in electron cryo-tomography (cryo-ET) have begun to open windows into the cell for investigating biological process in their native environment.[14,15]

Here, we introduce a sample preparation method cryoEM based on microfluidic atomic force microscopy (AFM)[16] that enables direct extraction of a small (femtoliter) volume from a cell in the form of a targeted subcellular biopsy, followed by dispensing this volume onto an electron microscopy grid and subsequent vitrification.

2. Setup Design

2.1. General Concept

The general idea of our sample preparation setup is to use a microfluidic AFM cantilever probe for taking a subcellular biopsy, dispensing the sample on an electron microscopy grid, and subsequent vitrification. We abbreviate this process as AFM4cryoEM. The entire sample preparation process is enclosed in an environmental chamber kept at 70% humidity, while the transmission electron microscopy (TEM) grid is maintained just above the dew point to avoid evaporation from, or condensation on the dispensed droplet. The advantages of using a microfluidic AFM cantilever over other approaches for small volume manipulation of cellular material are the ability to obtain force feedback in real-time during the biopsy process, the scalable production of probes, and the design freedom for probes.[17,18] A schematic of the setup is shown in **Figure 1**.

2.2. Sample Preparation Workflow

The sample preparation process is divided into three consecutive phases, Phase A: Grid loading, Phase B: Aspiration/Dispensing, and Phase C: Vitrification, as shown in **Figure 2**. The major components of the setup are shown in Figure 2-A1: inverted fluorescence microscope, microfluidic AFM cantilever, translation stage, humidity chamber, plunger with tweezers, and the sample (here represented by a cell). Prior to starting the sample preparation, cells grown on coverslips and maintained in growth medium are loaded onto the stage, and the subcellular target for aspiration is identified by fluorescence microscopy. The grid holder and the coverslip with cells are mounted on an x-y translation stage driven by a piezoelectric actuator. In **Phase A**, a plasma-treated grid is mounted on the tweezers and moved into the humidity chamber through an entry/exit port (Figure 2-A2). The stage is moved to bring the grid holder under the tweezers clamping the grid. The grid holder is rotated by 90 degrees anticlockwise to receive the grid from the tweezers. The alignment of the grid with the grid holder is crucial to avoid collision of the grid while loading inside the grid holder. The tweezers are then moved down to place the grid inside the grid holder (Figure 2-A3), release the grid and moved up to clear the path. The grid holder is rotated by 90 degrees clockwise and clamps the grid. The grid is maintained slightly above the dew point using a Peltier element (Figure 2-A4). In **Phase B**, the stage with grid and sample are moved under the AFM for fluorescence-based target selection using the fluorescence microscope. The microfluidic AFM probe that is pre-filled with buffer is used for subcellular extractions (Figure 2-B1). The force curve of the AFM while approaching the target cell or substrate is used as real-time feedback to guide the cantilever interaction with the cell and the substrate surface. Once the cell is punctured and the desired target region inside the cell is reached, underpressure is applied inside the tubing connected to the hydrophobic microfluidic AFM cantilever to aspirate the targeted subcellular volume. After the sample is aspirated, ambient pressure inside the tube is restored and the cantilever is retracted from the culture medium. The stage is moved to bring the TEM grid into the field of view of the optical microscope. Again, using the force feedback from the AFM, the cantilever is approached to the grid surface. After reaching the grid surface, a positive pressure is applied inside the tubing connected to the microfluidic AFM cantilever to dispense the aspirated volume onto the grid (Figure 2-B2). In **Phase C**, the stage is

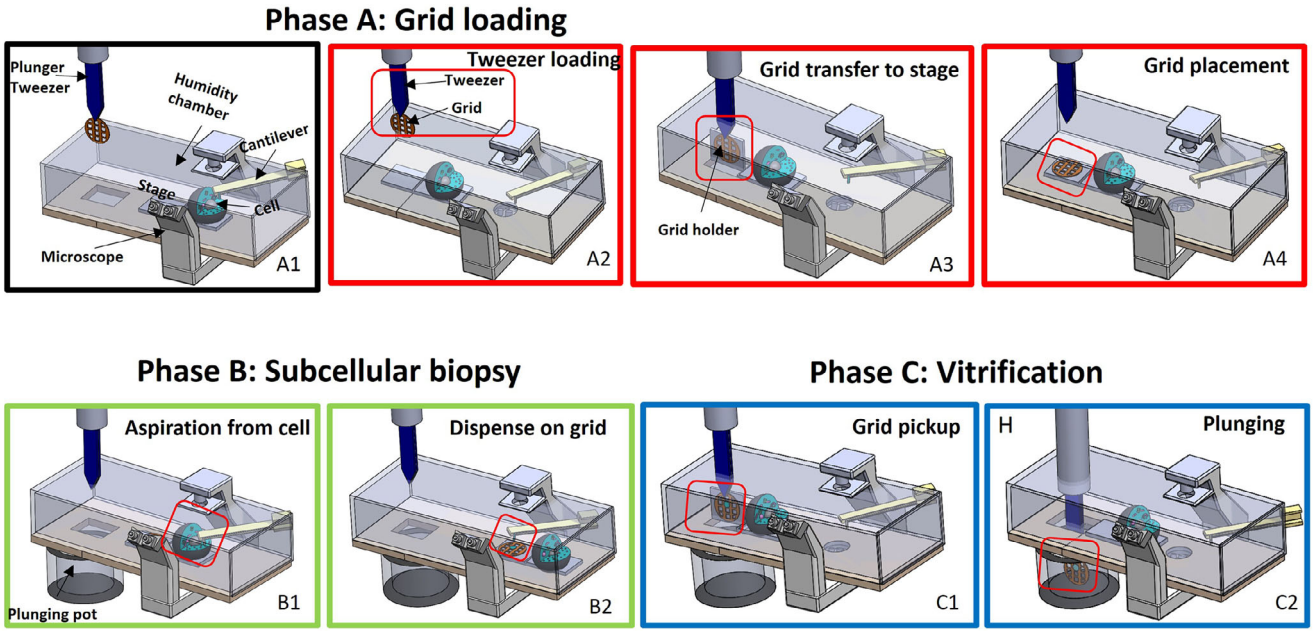

Figure 2. Critical moments of the AFM4cryoEM sample preparation process.

returned to the starting position to bring the grid holder below the tweezers. The grid holder is rotated by 90 degrees to allow grid pickup by the pre-mounted tweezers (Figure 2-C1). The stage clears the path for the plunger to pass through the entry/exit port of the humidity chamber. The port is opened, and the grid is plunged into liquid ethane located underneath the stage (Figure 2-C2). See Video S1 (Supporting Information) for the animation of the sample preparation workflow.

3. Results and Discussion

3.1. Setup

A rendered model and the corresponding photograph of the setup is shown in **Figure 3A,B**. The setup comprises four main units: microscopes (optical and AFM), XY stage, plunger, and humidity chamber. a) Microscopes: The AFM head was mounted on a custom-designed XY stage placed above an inverted optical fluorescence microscope. The subcellular target was monitored using the optical microscope. A microfluidic AFM cantilever was mounted on the AFM head and the pressure inside the cantilever was controlled by an external pressure controller ranging from 8 bar above the atmosphere to 1 bar below the atmosphere. b) Stage: The XY stage was fitted with a TEM grid holder connected to a peltier controller and a glass plate with cells in buffer. The cells or TEM grid were brought into the field of view of the optical microscope by moving the XY stage, Figure 3C. The stage had a resolution of 100 nm and a range of 50 cm in x-axis and 2 cm in y-axis. The grid holder made out of high-thermal conducting oxygen-free copper block was cooled with a peltier element to maintain the temperature at the dew point to prevent evaporation of the dispensed femtoliter volumes. The grid holder can rotate 90 degrees to stay horizontal on the stage for sample dispensing or vertical for the tweezers mounted on the plunger to pickup/release from/into the grid holder. c) Plunger: The vertical motion of the plunger was obtained by a linear motor, Figure 3D. The plunger was mounted with custom-made tweezers with automated opening or closing to release or hold the TEM grid respectively. For vitrification, a constant plunging speed of 1.5 ms^{-1} was used. d) Humidity chamber: The AFM head, XY stage, and the plunger were enclosed in a humidity chamber that was maintained at 70% relative humidity. The entire sample preparation process described in Figure 2 was automated using LabVIEW software (see Sections S.1.1 to S.1.3, Supporting Information).

3.2. Microfluidic AFM Cantilever

Aspiration and dispensing of femtoliter volumes was achieved by using a force-sensitive microfluidic cantilever mounted on the AFM head. The fabrication process of the silicon nitride microfluidic cantilever chip is described elsewhere.[19] The microfabricated chip is shown in **Figure 4A**, with the microfluidic AFM cantilever chip linked to an on-chip fluid reservoir (not visible in the figure, but situated on the rare side of the chip). The on-chip reservoir was connected to an external pressure controller. The cantilever is shown in Figure 4B, where the dots represent the pillars used to separate the top and bottom membranes of the microfluidic channel. The cantilever measures 200 µm in length, 36 µm in width, with a 1 µm channel height and 0.1 µm silicon nitride wall thickness, with a stiffness of 2 Nm^{-1}. The cylindrical cantilever tip of 5 µm long and a 1.5 µm nominal diameter is shown in Figure 4C. A corner lithography technique[20] was used to fabricate four nanowires meeting at a point to create a sharp tip.

The microfluidic AFM cantilever was glued to a fluidic interface and connected to an external pressure controller. The tall tip facilitates a uniform incision into the cell, and a wide

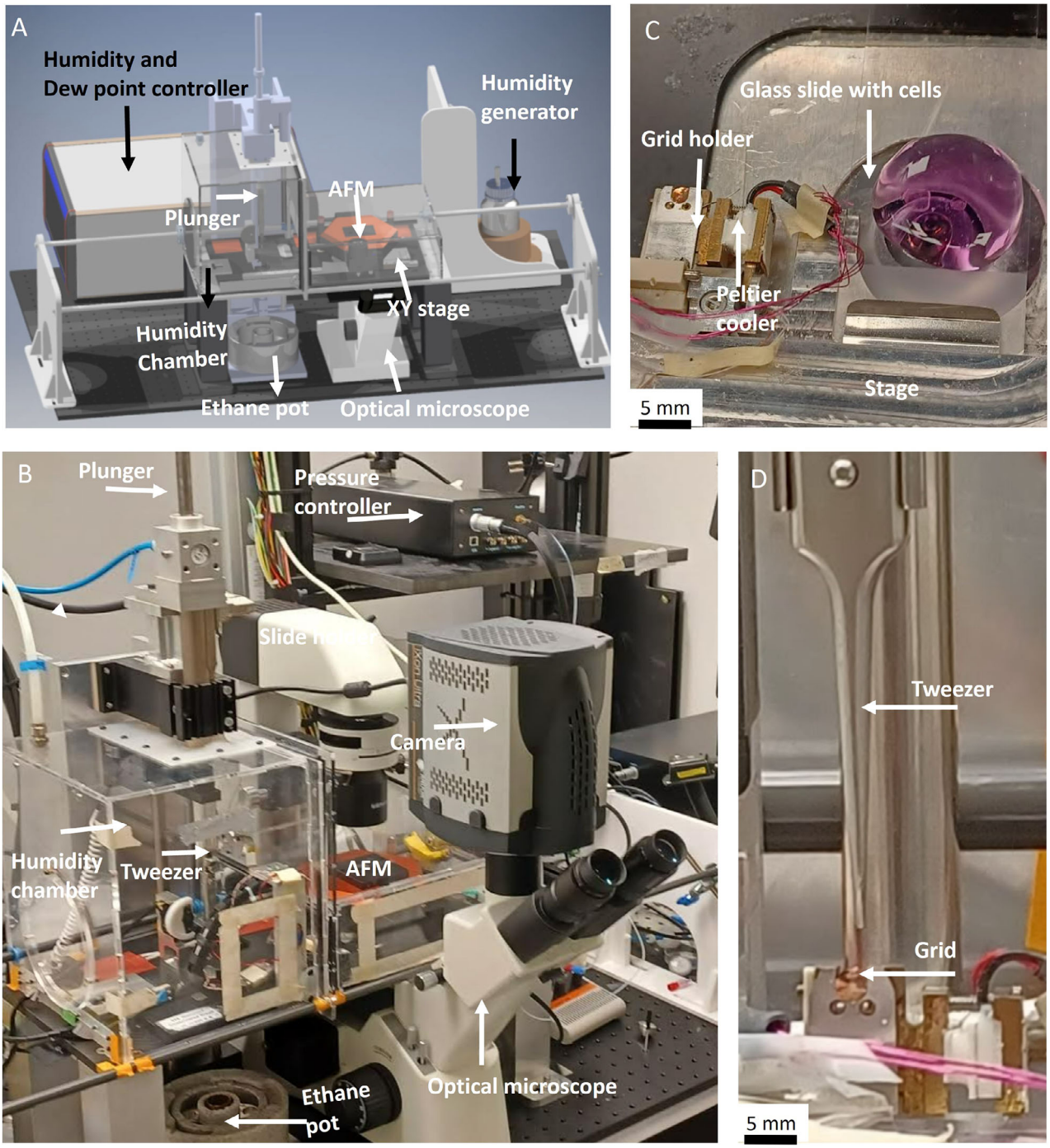

Figure 3. The AFM4cryoEM setup. A) A rendered model of the setup. B) Photograph of the setup. C) XY stage with sample holder and grid holder kept at dew point temperature using a peltier element. D) Plunger with tweezers shown in the process of releasing a TEM grid into the grid holder.

aperture size minimizes clogging. Prior to the experiments, the cantilevers were made hydrophobic by forming hexyl trichlorosilane self-assembled monolayers on the surface. The other cantilevers used for some of the reported experiments had a pyramidal tip with aperture on one of the side walls of the tip; see Section S.1.4 (Supporting Information). All cantilevers used were 2 Nm^{-1} in stiffness.

3.3. Dispensing on an Electron-Microscopy Grid

We tested the setup by dispensing femtoliter volumes of deionised water on a TEM grid. The XY stage allows the microfluidic AFM cantilever to precisely target individual grid squares on a standard 3 mm diameter copper mesh finder grid, each containing 200 squares with a side length of 127 µm (**Figure** 5A).

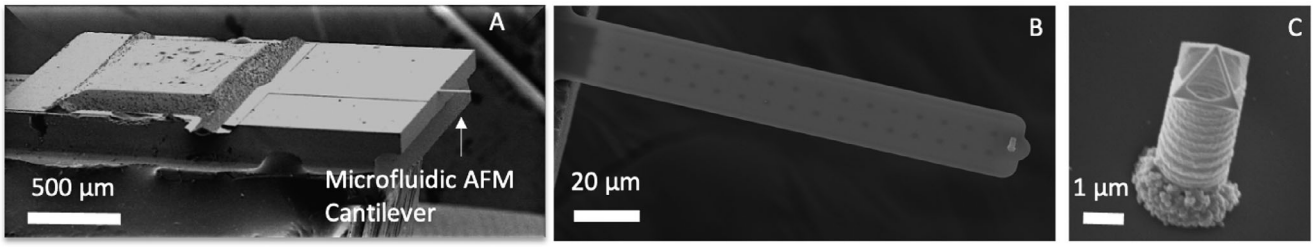

Figure 4. Scanning electron microscope image of the microfluidic AFM cantilever chip. A) Chip glued to the fluidic interface with arrow pointing to the location of the cantilever on the chip. B) Suspended microfluidic AFM cantilever. C) Cylindrical tip at the distal end of the cantilever with nanowires at the tip aperture.

These grids, marked for reference, aid in locating the sample in the electron microscope. The pressure applied to the fluid reservoir controls the amount of liquid dispensed onto each grid square. Before sample dispensing, the grid is plasma treated for 90 s to improve the wetting properties of the carbon film. To obtain the contact angle, TEM grid is glow discharged, and after waiting for the same time as it takes to mount and dispense on one grid square by the cantilever in the setup, a water droplet is placed on the carbon-side of the grid. It resulted in a contact angle of 40 °. This contact angle is used to calculate the volume of the dispensed droplets on the grid by measuring their actual diameter.

Applying pressures of 2 bar, 3 bar, and 4 bar for 5 s each over a pyramidal tip cantilever with a 1.5 µm diameter aperture on the tip, yielded dispensed volumes of 2.9 pL, 5.1 pL, and 10.5 pL, respectively (see Figure 5B–D). See Sections S.1.5 and S.1.6 (Supporting Information) for details on volume calculations. This demonstrates the capability to dispense individual droplets on multiple grid squares. It is noteworthy that the dispensed liquid volume is sufficiently small, forming distinct droplets, as opposed to layered dispersions observed when larger volumes are applied to the grid.[8] Improvements in maintaining hydrophilicity of the grid substrate surface may be required to generate liquid films sufficiently thin for phase-contrast imaging.

3.4. Dispensing on TEM Specimen Support Grids

To test dispensing and TEM imaging of biological macromolecules, we used the microfluidic cantilever to dispense several test samples through a 1.5 µm aperture pyramidal tip on the grid. First, we dispensed a high-contrast sample consisting of a 20 nm gold nanoparticle solution and imaged the grid after drying, **Figure 6A**. The particles showed an expected diameter and did not clog the cantilever. Next, we dispensed horse spleen apoferritin (ApoF), a dodecameric 450 kDa protein complex, at a concentration of 250 µg ml^{-1} that amounts to about 500 molecules per pL. After dispensing on the grid, the sample was stained with 0.2% uranyl acetate before imaging. The images showed particles consistent with the dimensions, and known ultrastructural appearance of ApoF (Figure 6B).[21,22] To test the compatibility of the microfluidic cantilever with soft biological objects, we also dispensed unilamellar liposomes with an average diameter of 105 nm (range: 50 to 300 nm) made from a total lipid concentration of 0.1 mg mL^{-1}. See Section S.1.7 (Supporting Information). TEM images of a negatively stained liposomes revealed a characteristic of collapsed and dehydrated state as shown in Figure 6C. While a tip aperture of 1.5 µm should be sufficiently wide for a liposome preparation of 300 nm maximum diameter, negative stain imaging is inconclusive as to whether a significant fraction of

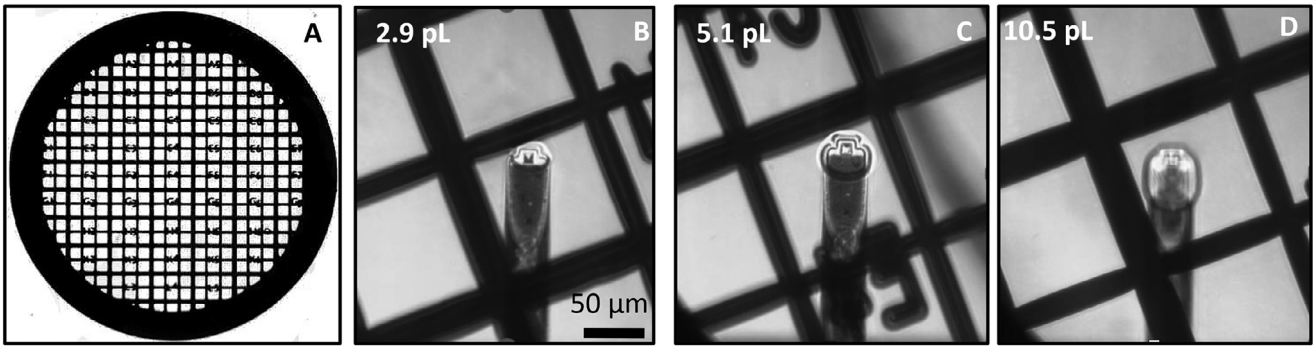

Figure 5. Dispensing deionised water on an electron microscopy grid. A) An overview image of a 3 mm diameter and 100 µm thick copper mesh TEM finder grid with continuous carbon film on which the sample is dispensed. B) A 2.9 pL volume dispensed with a droplet diameter of 34 µm. C) A 5.1 pL volume dispensed with a droplet diameter of 41 µm. D) A 10.5 pL volume dispensed with a droplet diameter of 52 µm. A contact angle of 40° was used to calculate the dispensed volume. See Sections S.1.5 and S.1.6, and Videos S2a–c (Supporting Information).

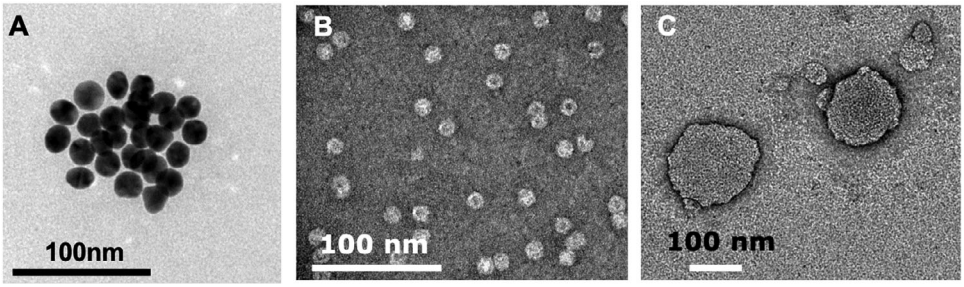

Figure 6. TEM images of the dispensed samples. A) Gold nanoparticles, B) Negatively stained Apoferritin, C) Negatively stained liposomes.

liposomes are ruptured during the aspiration or dispensing process.

3.5. Single Cells and Force Feedback

Having established the dispensing capability of hard and soft nanometer scale objects on the grid, we next tested the setup for cytoplasmic injections and extractions. The access to the cytoplasm was achieved by piercing the sharp hollow cantilever tip into the targeted cell. By applying over- or under-pressure using the microfluidic pressure controller, liquid material was injected into or extracted out from the cytoplasm.[23] The force feedback obtained from the microfluidic cantilever gave a real-time information on subcelluar location during penetration. Force-distance curves collected at three locations—on the nucleus, perinuclear region, and the edge of the cell, are shown in **Figure 7**. Locations for approach of the cantilever probe were chosen using the optical microscope integrated in the setup. The slope of the force curve indicates the level of reaction force from the surface. The force curve taken on the nucleus, which is typically the tallest region of a cell, shows more indentation depth (approximately 8 µm) with forces increasing gradually with distance as shown in Figure 7A. The force curve on the perinuclear region showed a puncturing event at a force of 2 nN, Figure 7B. The steep slope in the force curve taken at the edge of the cell, as shown in Figure 7C, indicates the microfluidic AFM cantilever tip was touching the hard surface of the glass substrate underneath the cell. These force curves were obtained using a pyramidal tip probe with an 1 µm diameter aperture. Cylindrical tip probes also produce similar force curves. A kink in the force curve during cell membrane penetration was not reproducible during every penetration event by either probe tip, indicating further optimization of the probe tips is needed. Results from others using solid AFM tips indicate taller tips are more suited for recording cell membrane penetration events.[24] Force curves obtained on other cell types are given in the Section S.1.8 (Supporting Information).

3.6. Subcellular Injection

To demonstrate targeted injection of liquids inside a single-cell, a fluorescence dye (fluorescein) was injected inside the cell using cylindrical tip cantilever. The injected cell swells in volume, indicating a successful injection inside the cell before it bursts due to excess pressure. Different

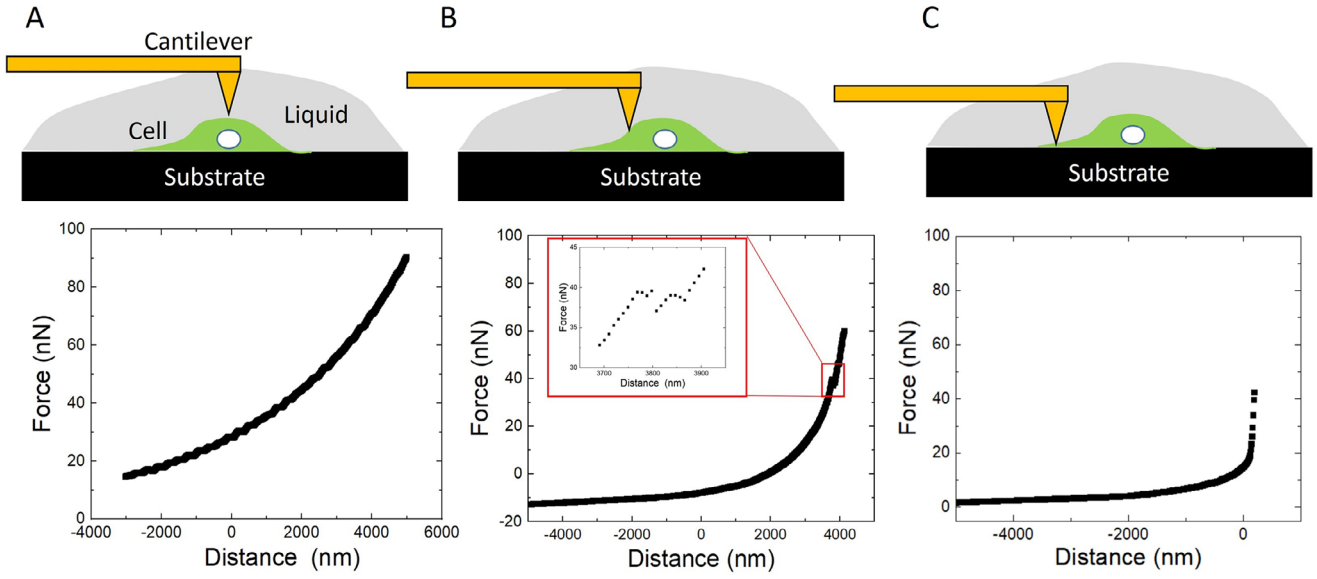

Figure 7. Force feedback from the microfluidic cantilever during a subcellular biopsy. Force-distance curves are shown for cantilever approaches A) at the center of the cell, B) near the perinuclear region, C) at the edge of the cell.

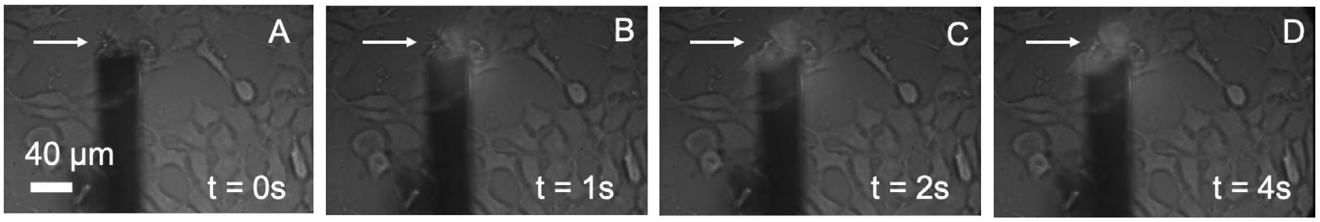

Figure 8. The injection of fluorescent dye into a single cell is shown. The arrow indicates the bulging of the cell over time as the liquid is injected, Video S3 (Supporting Information).

time points of injection are shown in **Figures 8A–D**. The video of the same can be seen in the Video S3 (Supporting Information).

3.7. Subcellular Biopsy for cryoEM Sample Preparation

Cytoplasmic content extraction experiments were done on HeLa cells. A force setpoint between 50 to 100 nN was used to approach and puncture the cell. After puncture, an underpressure of 800 mbar below atmosphere was applied inside the cantilever, resulting in an aspiration of the cytoplasmic contents inside the fluidic channel. Various moments during cytoplasmic extraction as observed by the inverted optical microscope of the setup are shown in **Figures 9A–C** indicated by the meniscus inside the cantilever. See Video S4 (Supporting Information). Note that the cantilever is prefilled with buffer solution upto the tip aperture. Liquid upto the tip aperture is maintained by continuously applied slight positive pressure of tens of millibar by the pressure controller while the cantilever is in air environment. As soon as the positive pressure is removed, liquid near the cantilever probe tip evaporates creating an air gap inside the cantilever. Such a probe with an air gap near the tip is used to aspirate the subcellular contents of a cell. During aspiration, a liquid meniscus can be seen with an air gap between the aspirated content and the buffer inside the cantilever microfluidic channel. The process of air gap creation

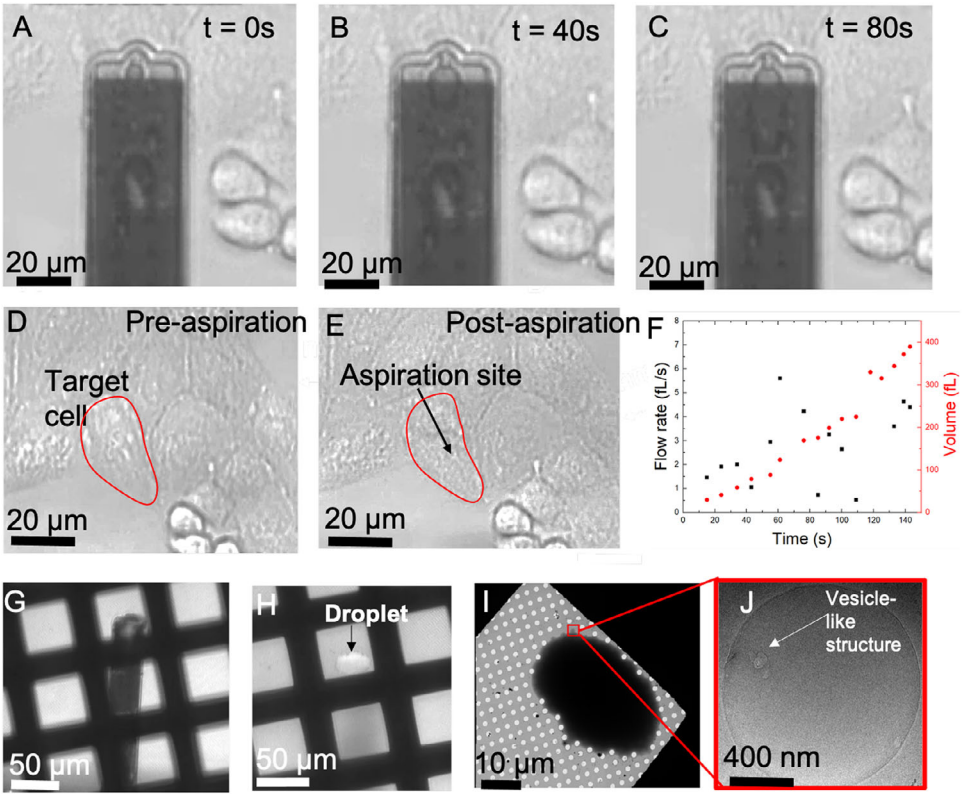

Figure 9. Single cell biopsy and corresponding cryoEM images. Optical microscopy images at different time points with the cantilever in contact with the target cell and movement of meniscus inside the cantilever at the A) beginning of aspiration, B) mid-aspiration, C) end of aspiration, see Video S4 (Supporting Information). D) Target cell prior to cytoplasmic extraction, E) Target cell after cytoplasmic extraction, F) Aspiration flow rate and the volume collected with time measured from Video S4 (Supporting Information). G) Optical microscopy image during dispensing on the grid. H) Optical microscopy image after dispensing. I) Correlated magnified cryoEM micrograph of the dispensed droplet shown in Figure H. J) Higher magnification micrograph of grid hole located at the droplet periphery.

also avoids diffusion or dilution of the extracted content with the buffer inside the cantilever. Pre-and post-aspiration images of the cell are shown in Figure 9D,E, respectively. The approximate volume aspirated after 150 s was ≈450 fL. The flow rate and volume variation with time is shown in Figure 9F. The flow rate was not constant as there is an irregular wetting pattern. The irregular shape of the meniscus was due to the support pillars inside the cantilever that acts like phase guide for liquid movement. Effectively, there was a mean flow rate of 2.5 fLs^{-1} with a standard deviation of 1.9 fLs^{-1}. Cantilevers with cylindrical tip yielded more consistent results with a low probability of clogging compared to pyramidal tip with 600 nm aperture on the side for cytoplasmic extraction.

After aspirating the cell content, the cantilever was retracted, the stage was moved to bring the grid into the field of view of the optical microscope just below the cantilever probe with aspirated content. To dispense the contents, the cantilever probe tip was approached towards the suspended carbon foil within a chosen grid square, Figure 9G. As the tip touched the carbon foil, an over pressure of 1 bar above atmosphere was applied for 10 s to release the cantilever contents on the grid square. The droplet dispensed on the grid is shown in the optical microscopy image Figure 9H, ≈5.1 pl in volume. See Section S.1.9 (Supporting Information). This resulted in about eleven times dilution of the 450 fL aspirated content. The grid with cellular content dispensed was vitrified by plunge freezing in liquid ethane. cryoEM micrographs of the grid square containing the cytoplasmic extract are shown in Figure 9I. The wet droplet image obtained from optical microscopy after dispensing and vitrified droplet image in cryoEM are correlated. Due to insufficient droplet spreading most areas were too thick for transmission electron imaging. Micrographs taken over grid holes with the thinnest areas at the droplet edges show some vesicle-like structures (Figure 9J), but the low contrast due to excessive ice thickness precludes conclusive interpretation. We need further experiments to improve droplet spreading across the perforated support film in order to yield areas sufficiently thin for high-contrast imaging and for conclusive evidence that cytoplasmic content can be successfully extracted and dispensed using our setup. Possible approaches toward this goal could be (a) acceleration of the workflow to minimise the time between glow discharing and dispensing for better droplet spreading, integration of real-time thickness measurements in the setup, or (c) combining the cantilever-based extraction with nanofluidic cryoEM sample supports featuring fixed channel heights, as shown in Ref. [13].

3.8. Femtolitre Dispensing of Single-Particle cryoEM Samples

To assess the cryogenic workflow of femtolitre dispensing for cryoEM sample preparation we used tobacco mosaic virus (TMV) as a test specimen. For dispensing TMV, the cantilever was prefilled with 3 mg mL^{-1} of TMV solution from the fluidic interface reservoir with the pressure system. The stage was moved into the grid observation position in the field of view of the optical microscope. Subsequently, the cantilever was advanced towards a selected grid square until the contact is established as judged from the force-distance curve. A droplet was dispensed using a positive pressure of 1 bar for around 3–10 s. Subsequently, the cantilever was retracted and moved to a new grid square for a new dispensing step. Since the dew point control prevents rapid evaporation, dispensing series of droplets in several separate grid squares was possible. In this case, three individual droplets were dispensed on three separate grid squares (see Video S5, Supporting Information). Eventually, the grid was plunge frozen and transferred to a cryoEM for imaging. The optical microscopy image of three dispensed droplets in three separate grid squares is shown in **Figure 10A**, the corresponding correlated cryoEM montage of the entire grid and the dispensed droplets are shown in Figures 10B–F. The smallest droplet is shown in Figure 10F and contains approximately 204 fL, and all dispensed volumes are in the range of hundreds of femtolitres. These volumes are at least two orders of magnitude lower than previous results reported in Refs. [13, 25, 26], which are in the pL or nL range of effective sample usage. In the present case, the effective volume was computed by approximating the circular footprint of a droplet whose contact area with the grid is given by the red circle as marked in the Figure 10D–F. A contact angle of 40° was used for the calculation. See Sections S.1.5 and S.1.6 (Supporting Information). This approximation is conservative as it considers a larger contact surface of the droplet than that experimentally found in the cryoEM micrographs. As judged from the overview images, droplet spreading was poor and only very few grid holes showed ice thickness compatible with TEM single-particle imaging.

We next acquired high magnification images of vitrified TMV samples in suitably thin areas, as shown in **Figure 11A** (TMV, see Video S6, Supporting Information) While high magnification micrographs of TMV droplets revealed intact virions consistent with the typical axial dimension of ≈ 300 nm and a width of 18 nm, the thick ice (minimal thickness > 100–140 nm) required imaging at high defocus to visualize the virions and the limited number of usable foil holes precluded averaging and 3D reconstruction (Figure 11B–F; Section S.1.10, Supporting Information). Our results demonstrate that biological macromolecules can be aspirated and dispensed without obvious damage, but suggest that further optimization is required to ensure uniform spreading of femtolitre droplets into thin films across perforated support films.

4. Conclusion

In conclusion, we have developed a system capable of precisely dispensing volumes as small as about 204 fL onto a support grid for vitrification and cryoEM imaging. We demonstrated controlled dispensing of femtoliter droplets containing TMV, confirming that the TMV virions remain structurally intact during cryoEM imaging. Additionally, our setup enables the extraction and dispensing of subcellular material from single cells. When combined with the integrated fluorescence microscope, this system lays the foundation for targeted subcellular biopsies for cryoEM analysis.

Our data suggest that further improvements are needed in droplet spreading and evaporation to consistently generate thin vitreous layers suitable for imaging. This goal can likely be achieved through mechanical design enhancements that accelerate the time between dispensing and plunging, eliminating the need for the current slow piezoelectric stage used for sample translation.

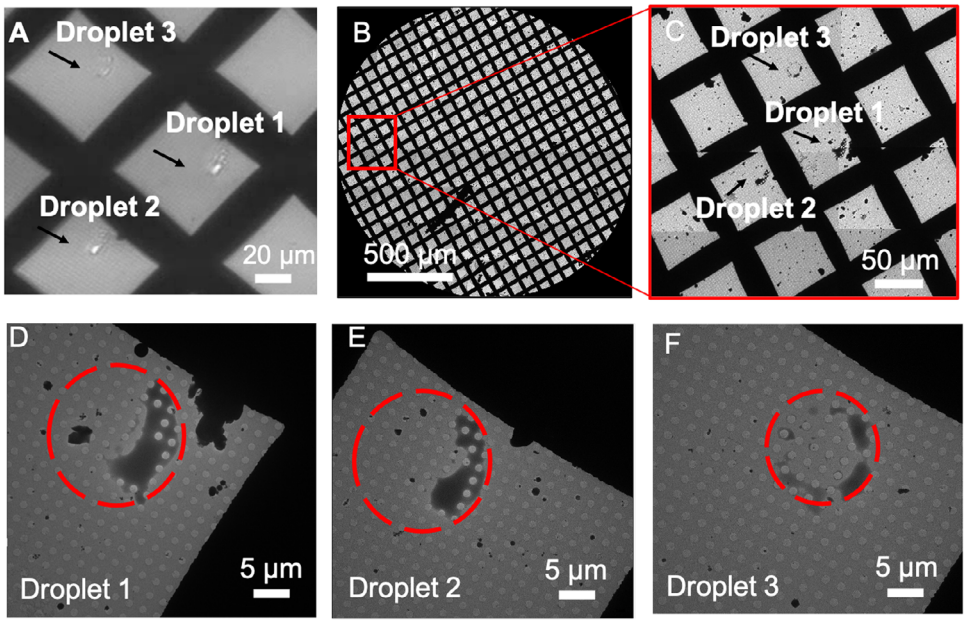

Figure 10. Micrographs showing the dispensing capability of the setup. A) Optical microscopy image showing the grid squares with the location of the dispensed droplets, see also Video S5 (Supporting Information). B) cryoEM montage of the entire grid. C) Close-up of the montage showing the dispense location. D–F) Medium magnification micrographs of grid squares containing the individual dispense locations. The volume for each of the droplets were 435, 366, and 204 fL, respectively, with the corresponding diameters being 18 µm, 17 µm, 14 µm. respectively.

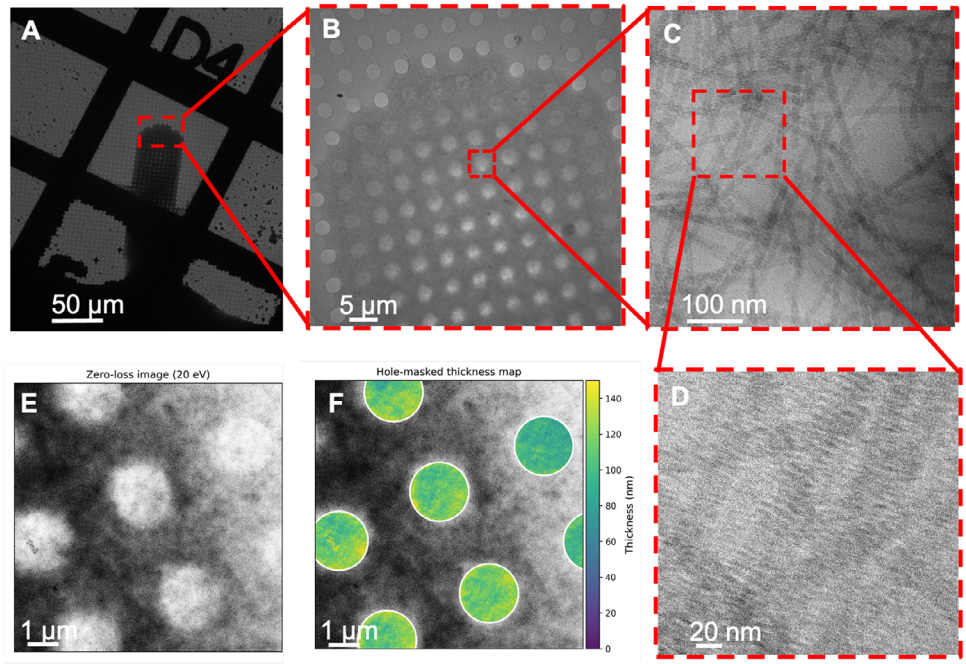

Figure 11. CryoEM Micrographs showing the cryoEM images obtained by dispensing a concentrated solution of tobacco mosaic virus (TMV) on R2/2 grids. A) CryoEM montage showing the grid square with dispensed droplet. B) Medium magnification micrograph of the foil holes at the droplet edge. C) High magnification micrograph of suspended TMV in foil hole. D) Close-up of the region indicated by dotted box from figure C. E) Energy-filtered zero-loss micrograph acquired with a 20 eV slit. F) Thickness map superposed onto the zero-loss micrograph; the mask is on the foil holes. See Video S6 (Supporting Information) for TMV dispensing.

While our results show that subcellular aspiration and the subsequent dispensing of cytoplasmic content are technically feasible, additional refinements to the cantilevers and setup are required for conclusive evidence of targeted extraction and routine experiments. We are actively working towards achieving these improvements.

5. Experimental Section

Microfluidic Cantilevers: The microfluidic cantilevers were fabricated by Smarttip in The Netherlands. These cantilevers had a spring constant of 2 Nm^{-1} and featured pyramidal and cylindrical tips, with apertures measuring 1.5 µm in nominal diameter. Additionally, pyramidal-tip and tipless microfluidic cantilevers from Cytosurge AG were occasionally used for the experiments.

Functionalization: The fabricated cantilevers were placed in a closed Petri dish containing a container with 40 µL of octyl trichlorosilane. The silane vapors formed a surface-assembled monolayer on the cantilever surface, rendering it hydrophobic within 10 min.

Fluidic Interface: The microfabricated cantilever was affixed to a custom 3D-printed plastic fluidic interface using Loctite 9492 epoxy adhesive. The fluidic interface was printed with an EnvisionTec printer. A silicone tube was then attached to the interface to deliver liquids to the microfluidic cantilever and was connected to a pressure controller for precise flow control.

Pressure Controller: During the experiments, fluid flow was controlled using either the Elveflow or Cytosurge CORA pressure controllers. The Elveflow pressure controller allowed pressure to be varied from 800 mbar below atmospheric pressure (vacuum) to 8 bar above atmospheric pressure, while the Cytosurge CORA controller had a pressure range from 800 mbar below atmospheric pressure to 1 bar above atmospheric pressure. A Rheodyne fluid selector was used to switch between pressure channels.

Clog Test: After gluing, the cantilevers were tested with air to check for any potential clogging. A 1 mL syringe filled with ambient air was attached to the silicone tubing connected to the fluidic interface, and pressure was applied manually to the plunger. If a clog was present, the plunger would remain stationary over time. In the case of a leak (such as at the glue joints or a break in the microfluidic channels), the plunger would move easily, displacing all the air. For a perfectly sealed and unclogged cantilever, the plunger would move very slowly due to the significant resistance caused by the 1.5 µm aperture of the cantilever tip. The deionized water used for experiments was two times filtered with a a 100 nm pore size to avoid any clog due to particle contamination.

Microscopes: A Motic AE32 inverted optical fluorescence microscope, equipped with an iXon Ultra CCD camera and long-working-distance objectives, was used for imaging. For atomic force microscopy (AFM), a Nanosurf AG FlexFM was employed, controlled by a C3000 controller, featuring a custom-modified cantilever holder designed to accommodate the 3D-printed fluidic interface. Additionally, Cytosurge AG's commercially available FluidFM holder and cantilevers for Nanosurf AFM were used in some experiments.

XY Stage: A thermally insulating carbon fiber plate, mounted on the optical microscope and equipped with both an XY stage and an AFM stage, was designed and fabricated by Nanosurf AG. The precision XY stage from SmarAct GmbH with precision position controllers was used for accurate movement. The stage included a glass slide holder for cells and a temperature-controlled TEM grid holder, regulated by a local Peltier element. The AFM head, with the cantilever securely clamped onto the AFM holder, was positioned on the AFM stage.

Negative Staining: The TEM grids were glow discharged for 90 s before being used with the microfluidic cantilever for dispensing. The samples were allowed to dry, after which 0.5 µL of 0.2% Uranyl acetate was pipetted onto the grid and allowed to evaporate. Imaging was performed immediately afterward. The JEOL 1400 TEM was used to capture images of the negatively stained samples.

Cell Culture: HeLa cells stably expressing the mRFP-GFP-LC3 reporter construct (HeLa mRFP-GFP-LC3; kindly provided by Fulvio Reggiori, University of Aarhus, Denmark) were cultured in 90% Dulbecco's Modified Eagle Medium (DMEM), 9.9% Fetal Bovine Serum (FBS), and 0.1% Penicillin-Streptomycin (PS) on a three-well removable chamber glass slide (IBIDI) for 48 h at 95% humidity and 5% CO_2. The cells were then washed twice with PBS to remove any remaining culture medium. Next, warm starvation buffer (20 mM HEPES, 4-(2-hydroxyethyl)-1-piperazineethanesulfonic acid, pH 7.5, 140 mM NaCl, 1 mM $CaCl_2$, 1 mM $MgCl_2$, 10 mM glucose) was added to induce the formation of autophagosomes. Cells with fluorescently labeled autophagosomes after 30 min of starvation are shown in **Figure** 12.

Tweezers for TEM Grid: A commercially available DUMONT tweezer was cut into two halves, each with an initial tine width of 100 µm. The tines were then bifurcated into two separate parts and mounted onto a custom-designed holder as shown in **Figure** 13. The holder features a slot for securing the tweezers to the linear motor (used for plunging) via a screw. A circular gradient thickness plastic knob was used to control the opening and closing of the tines. The knob presses against a cam wheel, whose rotation gradually opens or closes the tines to release or grip the grid.

Humidity Chamber: The humidity chamber of the system was maintained at 37 °C and 70% humidity. Heating pads on the carbon fiber plate were used to regulate the temperature, while a humidity generator produced the necessary humidity. The humidity control system was developed by Maastricht University-IDEE. The accompanying software allowed for precise control of the humidity and temperature, ensuring the TEM grid was maintained near the dew point. Starting from room conditions (40% RH), the humidity in the chamber could be raised and stabilized to 70% at 37 °C, with the TEM grid kept near the dew point, within approximately 45 min

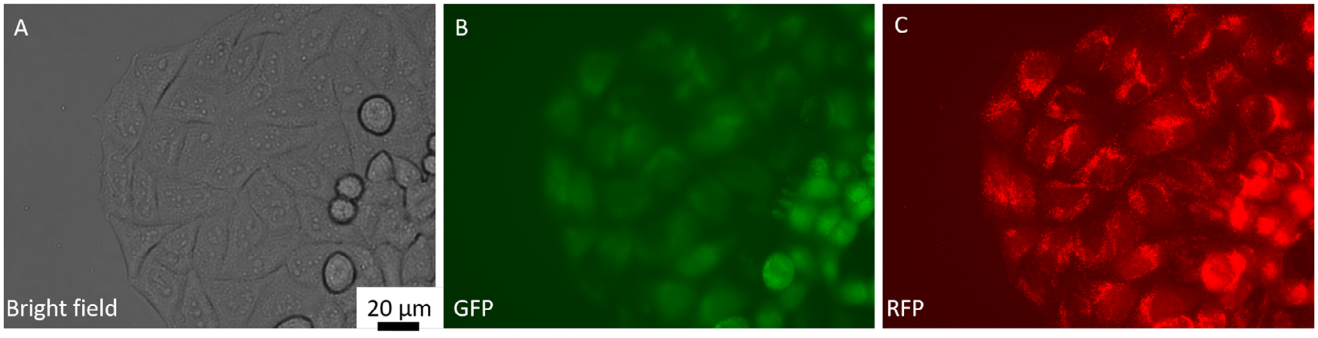

Figure 12. Optical microscopy images of cell culture taken before the experiments. Fluorescence image showing the autophagosomes after starvation. A) Bright field image B) Fluorescence image (GFP channel) C) Fluorescence image (RFP channel).

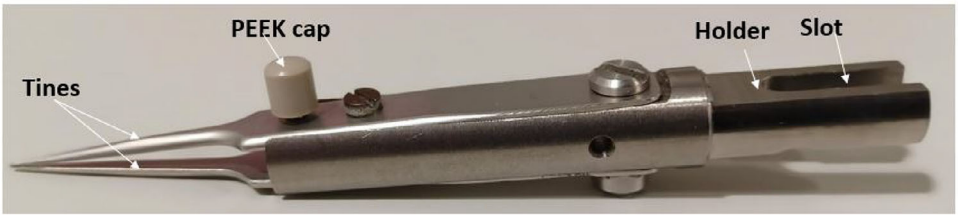

Figure 13. Photograph of the modified tweezer used in the setup.

LabVIEW Program: The setup includes various control components, such as micro-switches, servomotors, an XY stage, and a linear motor, all controlled by a LabVIEW program with a user-friendly front panel (see Section S.1.2, Supporting Information). Additionally, the humidity and pressure controllers each had their own dedicated LabVIEW programs.

Cryo-Electron Microscopy: CryoEM micrographs were acquired using a JEOL JEM3200-FSC cryo-transmission electron microscope system operated at 300 kV with a Gatan K2 summit detector at a magnification of 30,000× (1.288 Å/pixel) and an cumulative exposure of 50 $e^{-1}Å^{-2}$.95 s. Ice thickness was determined using energy-filtered transmission electron microscopy (TEM) by comparing the intensities of filtered and unfiltered images, following the method described by Ref. [27]. Measurements were performed with an in-column energy filter using a 20 eV slit, and thickness d was calculated using the equation:

$$d = \Lambda \cdot ln\frac{I}{I_{ZLP}} \quad (1)$$

where d is the ice thickness, I is the integrated total intensity, I_{ZLP} is the integrated zero-loss peak intensity, and Λ is the apparent mean free path for inelastic scattering in amorphous ice.

Supporting Information

Supporting Information is available from the Wiley Online Library or from the author.

Acknowledgements

V.S., J.P., and E.V., contributed equally to this work. This work was part of the research project NFP4cryoEM (project number 13711), which was partially funded by the Netherlands Organization for Scientific Research - Stichting voor de Technische Wetenschappen (NWO - STW). A.J. acknowledged support from the European Research Council (ERC-StG-852880) and the Dutch Research Council (NWO.STU.018-2.007). The authors would like to thank Cecilia de Agrela Pinto and Jelle Mens for their assistance with cell culture and TMV dispensing experiments, respectively. The authors also acknowledged the co-operation of Cytosurge A.G. Additionally, the authors gratefully recognized the invaluable contributions of the late Jelle van der Does, whose work was instrumental in enabling many of the mechanical engineering designs incorporated into the setup.

Conflict of Interest

The authors declare no conflict of interest.

Data Availability Statement

The data that support the findings of this study are available from the corresponding author upon reasonable request.

Keywords

atomic force microscopy (AFM), cryoEM, femtopipette, FluidFM, microfluidic AFM cantilever, subcellular biopsy

Received: June 22, 2025
Published online:

[1] E. Nogales, *Nat. Methods* **2016**, *13*, 24.
[2] H. R. Saibil, *Mol. Cell* **2022**, *82*, 274.
[3] T. Nakane, A. Kotecha, A. Sente, G. McMullan, S. Masiulis, P. M. Brown, I. T. Grigoras, L. Malinauskaite, T. Malinauskas, J. Miehling, T. Uchanski, L. Yu, D. Karia, E. V. Pechnikova, E. de Jong, J. Keizer, M. Bischoff, J. McCormack, P. Tiemeijer, S. W. Hardwick, D. Y. Chirgadze, G. Murshudov, A. R. Aricescu, S. H. Scheres, *Nature* **2020**, *587*, 152.
[4] G. Weissenberger, R. J. Henderikx, P. J. Peters, *Nat. Methods* **2021**, *18*, 463.
[5] Z. Lu, T. R. Shaikh, D. Barnard, X. Meng, H. Mohamed, A. Yassin, C. A. Mannella, R. K. Agrawal, T.-m. Lu, T. Wagenknecht, *J. Struct. Biol.* **2009**, *168*, 388.
[6] S. A. Arnold, S. Albiez, A. Bieri, A. Syntychaki, R. Adaixo, R. A. McLeod, K. N. Goldie, H. Stahlberg, T. Braun, *J. Struct. Biol.* **2017**, *197*, 220.
[7] A. J. Noble, V. P. Dandey, H. Wei, J. Brasch, J. Chase, P. Acharya, Y. Z. Tan, Z. Zhang, L. Y. Kim, G. Scapin, M. Rapp, E. T. Eng, W. J. Rice, A. Cheng, C. J. Negro, L. Shapiro, P. D. Kwong, D. Jeruzalmi, A. D. Georges, C. S. Potter, B. Carragher, *eLife* **2018**, *7*, https://doi.org/10.7554/eLife.34257.
[8] R. I. Koning, H. Vader, M. van Nugteren, P. A. Grocutt, W. Yang, L. L. Renault, A. J. Koster, A. C. Kamp, M. Schwertner, *Nat. Commun.* **2022**, *13*, 1.
[9] T. Jain, P. Sheehan, J. Crum, B. Carragher, C. S. Potter, *J. Struct. Biol.* **2012**, *179*, 68.
[10] R. B. Ravelli, F. J. Nijpels, R. J. Henderikx, G. Weissenberger, S. Thewessem, A. Gijsbers, B. W. Beulen, C. López-Iglesias, P. J. Peters, *Nat. Commun.* **2020**, *11*, 1.
[11] T. S. Levitz, M. Weckener, I. Fong, J. H. Naismith, *Front. Mol. Biosci.* **2022**, *9*, 1.
[12] L. Rima, M. Zimmermann, A. Fränkl, T. Clairfeuille, M. Lauer, A. Engel, H. A. Engel, T. Braun, *Faraday Discuss.* **2022**, *240*, 55.
[13] S. T. Huber, E. Sarajlic, R. Huijink, F. Weis, W. H. Evers, A. J. Jakobi, *eLife* **2022**, *11*, 1.
[14] W. Baumeister, *Cell* **2022**, *185*, 2649.
[15] F. J. Bäuerlein, W. Baumeister, *J. Mol. Biol.* **2021**, *433*, 20.
[16] A. Meister, M. Gabi, P. Behr, P. Studer, J. Vörös, P. Niedermann, J. Bitterli, J. Polesel-Maris, M. Liley, H. Heinzelmann, T. Zambelli, *Nano Lett.* **2009**, *9*, 2501.
[17] R. C. Kramer, E. J. Verlinden, L. Angeloni, A. Van Den Heuvel, L. E. Fratila-Apachitei, S. M. Van Der Maarel, M. K. Ghatkesar, *Lab Chip* **2020**, *20*, 311.

[18] M. Blankespoor, T. Manzaneque, M. K. Ghatkesar, *Small Methods* **2024**, *8*, 2300942.
[19] H. H. P. Garza, *Development of Nanotools for Applications in (sub-) Femtofluidics and Graphene Technologies*. Ph.D. thesis, TU Delft, **2014**.
[20] E. J. Berenschot, N. Burouni, B. Schurink, J. W. Van Honschoten, R. G. Sanders, R. Truckenmuller, H. V. Jansen, M. C. Elwenspoek, A. A. Van Apeldoorn, N. R. Tas, *Small* **2012**, *8*, 3823.
[21] G. W. Richter, *J. Cell Biol.* **1959**, *6*, 531.
[22] W. H. Massover, *Micron* **1993**, *24*, 389.
[23] O. Guillaume-Gentil, R. V. Grindberg, R. Kooger, L. Dorwling-Carter, V. Martinez, D. Ossola, M. Pilhofer, T. Zambelli, J. A. Vorholt, *Cell* **2016**, *166*, 506.
[24] C. A. Lamontagne, C. M. Cuerrier, M. Grandbois, *Pflügers Archiv - Eur. J. Phys.* **2008**, *456*, 61.
[25] C. Schmidli, S. Albiez, L. Rima, R. Righetto, I. Mohammed, P. Oliva, L. Kovacik, H. Stahlberg, T. Braun, *Proc. Natl. Acad. Sci. U.S.A.* **2019**, *116*, 15007.
[26] V. P. Dandey, W. C. Budell, H. Wei, D. Bobe, K. Maruthi, M. Kopylov, E. T. Eng, P. A. Kahn, J. E. Hinshaw, N. Kundu, C. M. Nimigean, C. Fan, N. Sukomon, S. A. Darst, R. M. Saecker, J. Chen, B. Malone, C. S. Potter, B. Carragher, *Nat. Methods* **2020**, *17*, 897.
[27] W. J. Rice, A. Cheng, A. J. Noble, E. T. Eng, L. Y. Kim, B. Carragher, C. S. Potter, *J. Struct. Biol.* **2019**, *204*, 38.